Emotion-Dependent Functional Connectivity of the Default Mode Network in Adolescent Depression

Supplementary Information

Diagnostic Assessment of Subjects

The Schedule for Affective Disorders and Schizophrenia for School-Age Children-Present and Lifetime Version (K-SADS-PL) was administered to all potentially depressed adolescents. All K-SADS-PL diagnoses were verified by a board-certified child and adolescent psychiatrist (TTY). All depressed subjects in the study met full criteria for a current primary diagnosis of major depressive disorder (MDD) and were excluded from the study if they had a primary diagnosis of any other psychiatric disorder other than MDD. The computerized Diagnostic Interview Schedule for Children 4.0 (1) and the Diagnostic Predictive Scale (2) was used to screen for the presence of any Axis I diagnoses in the healthy control adolescents.

In addition to completing forms on basic demographics and general medical development, all subjects completed the following within three days of their scan session: Edinburgh Handedness Inventory (3), Customary Drinking and Drug Use Record (4), Family Interview for Genetics Studies (5), Ishihara Color Plates Test (8 plates, 2005 edition), Standard Snellen Eye Chart, Tanner Stage (6), and Wechsler Abbreviated Scale of Intelligence (WASI) (7). Parental socioeconomic status was measured using the Hollingshead Two Factor Index of Social Position (8).

Inclusion/Exclusion Criteria

All depressed subjects in the study met full criteria for a current primary diagnosis of MDD according to the DSM-IV and were excluded from the study if they had a primary

diagnosis of any other psychiatric disorder other than MDD. Exclusionary criteria for adolescents with MDD included left-handedness, prepubertal status (Tanner stage 1 or 2), being color blind or having less than 20/40 correctable vision, any contraindication to MR imaging (e.g., pregnancy, claustrophobia, metallic implants), a full scale IQ score < 80 (as measured by the WASI), a serious medical or neurological illness, a learning disability, the use of any medication with effects on the central nervous system within 2 weeks of their scan, substance abuse, evidence of illicit drug use or misuse of prescription drugs, and more than 2 alcoholic drinks per week or within the previous month at the time of scanning. All subjects but 5 were either actively engaged in cognitive behavioral therapy or family therapy consistently (n = 18) or had been at one point 3-4 years prior to the scan (n = 3). All depressed subjects were entirely naïve to antidepressants except for two: one had ceased medication usage 4 months before their scan and one had ceased 4 years before their scan. See Table 1 for a full summary of the clinical characteristics of our depressed subjects including comorbidities and Table S1 for a summary of psychosocial treatment history.

Healthy control (HCL) adolescents were excluded from the study for any of the exclusionary criteria for the depressed group, as well as any current or lifetime Axis I psychiatric disorder or any family history of mood or psychotic disorders in first- or second-degree relatives.

Three MDD subjects failed to complete the Ruminative Responses Styles (RRS), five depressed subjects could not provide an accurate age of illness onset, one healthy control failed to complete the Beck Depression Inventory-II (BDI-II), Multidimensional Anxiety Scale for Children, and RRS, and five other healthy controls failed to complete the RRS; these subjects were therefore excluded from all analyses involving these respective measures.

Six subjects (3 MDD) failed to have their button responses in the scanner recorded and were therefore excluded from final analyses.

Our fMRI analyses included rigorous motion and outlier thresholds. Volumes where the Euclidean norm of the motion derivatives exceeded 0.2 or where more than 10% of voxels exceeded the median absolute deviation of the detrended time-series were censored (see *Image Analysis* in the main text for more details). If more than 20% of the volumes within a single subject were censored, this subject was excluded from our final analyses. As a result, fourteen (8 depressed) subjects were excluded from the final whole brain and emotion-dependent functional connectivity analysis. We therefore report whole brain and emotion-dependent functional connectivity results for 63 subjects total: 26 adolescents with MDD and 37 HCL. For the resting-state data, we used a generalized least squares regression model that estimates the serial correlation of noise with an autoregressive moving average method. To control for the effects of physiological processes (cardiac, respiratory effects), we included the demeaned motion parameters, their derivatives, and the mean signal from white matter and cerebral spinal fluid as nuisance regressors into our model. Bandpass filtering ($0.01< f <0.1$) was also applied to the data via an inclusion of a series of sines and cosines into the regression model. This method of bandpass filtering, in addition to our nuisance regressors and our conservative censoring procedure (described above), therefore required a minimum number of time points for our regression model to successfully fit the time-series data. Subjects whose preprocessed resting-state data did not meet this minimum threshold of time points for appropriate model fitting were therefore excluded from further analysis. Consequently, the data from 7 participants (4 MDD and 3 HCL) were excluded. We therefore report resting-state results for 57 subjects. Exclusion rates did not differ significantly between groups: $\chi^2 = 0.429$, $p = 0.513$.

Experimental Stimuli and Paradigm

Emotional face stimuli have been shown to deactivate regions of the default mode network (DMN) in healthy individuals (9), making them the ideal stimuli to use to examine abnormalities in the DMN related to emotional processing. However, the only other functional connectivity study in adolescent depression using emotional face stimuli did not explicitly examine the DMN and only used static fearful faces in their emotional processing task (10). While fearful faces have been shown to elicit exaggerated responses in depressed versus healthy individuals (11, 12) and that this pattern reverses with successful treatment (13-15), there is also mounting evidence that depressed individuals exhibit differential responses to mood-incongruent stimuli such as happy faces (16) that is also modulated with successful treatment (17, 18). Moreover, there are at present no fMRI studies examining neural responses to sad faces in adolescents with depression (12). However, several studies have reported abnormal brain activation to sad faces in depressed adults (16, 19, 20) that normalizes with treatment (21-24) and predicts clinical remission (25), strongly suggesting that neural processing of sad stimuli may be especially relevant to depression. Finally, because dynamic face stimuli are considered more ecologically valid and more robustly activate facial affect processing regions compared to static face stimuli (26, 27) and because the only other functional connectivity study using face stimuli to examine adolescent depression used only static fearful faces (10), our emotion identification task employed dynamically morphing faces expressing fear, happiness, and sadness.

Our facial emotion identification task was adopted from a previously published PET paradigm (28), which was created and presented using an in-house Tcl script

(http://www.tcl.tk/software/tcltk/). Ten faces (5 female) from a standardized series of facial expressions of fear, happiness, and sadness (29) were morphed using computer graphical manipulation (28, 30). On Face trials, a screen displaying text of the three possible emotions to discern (Fear, Happy, Sad) was presented for 1500 ms. Next, a neutral face morphed in linear steps to an emotion of prototypical intensity over the span of 3000 ms. The face of maximal emotion then remained on the screen for an additional 800 ms of the trial before the screen turned blank for 700 ms (see Figure 1A in the main text). At stimulus onset, two possible emotion choices were displayed in text on the bottom left and right corners; subjects were instructed to press one of two buttons corresponding to the displayed emotion as soon as they recognized the emotion of the face. The pairs of possible emotion choices were: Happy versus Sad, Happy versus Fear and Sad versus Fear. As a sensorimotor control, we also had Oval trials (6 s per trial), where subjects had to determine if the top of an oval was tilting to the left or right and make a button response accordingly as soon as they recognized the tilt direction (see Figure 1B in the main text). The maximal angle of the oval tilt was 10°. At the end of the functional scan, a blank screen was presented for 10 s. In total, there were 80 trials (60 facial trials and 20 oval trials; total run = 490 s). Response time and accuracy on every trial during scanning was recorded.

Image Acquisition

All scanning was carried out on a General Electric 3T MR750 System (General Electric Healthcare, Milwaukee, WI) with Twin Speed gradients and a GE 8-channel head coil at the Center of Functional MRI at the University of California, San Diego. A fast spoiled gradient recalled sequence was used to collect T1-weighted images: TR = 8.1 ms, TE = 3.17 ms, TI = 450

ms, flip angle = 12°, 256 x 256 matrix, FOV = 250 x 250 mm, 168 sagittal slices 1 mm thick with an in-plane resolution of 0.98 x 0.98 mm. For the emotion identification task, T2*-weighted echo planar images (EPI) were acquired using the following pulse sequence: TR = 1000 ms, TE = 30 ms, flip angle = 90°, 64 × 64 matrix, FOV = 192 x 192 mm, 490 repetitions, 20 contiguous axial slices 3 mm thick with an in-plane resolution of 3 x 3 mm. For the resting-state scan, EPI images were acquired with the following pulse sequence: TR = 2000 ms, TE = 30 ms, flip angle = 90°, 64 × 64 matrix, FOV = 192 x 192 mm, 256 repetitions, 30 contiguous axial slices 3 mm thick with an in-plane resolution of 3 x 3 mm. Subjects lay supine in the bore of the magnet. During the task, they were instructed to relax but remain awake and as still as possible while making responses on a button box. During resting-state, subjects were instructed to look at a centrally presented white fixation cross and to keep as still as possible. Visual stimuli were projected onto a screen and viewed through a small, angled mirror mounted above the subject's head.

Emotion-Dependent Functional Connectivity (Psychophysiological Interaction [PPI]) Image Analysis

Individual raw time-series data underwent standard preprocessing (see *Image Analysis* in the main text), bandpass filtering ($0.009 < f < 0.08$), and motion outlier censoring. The mean preprocessed time-series from each seed was extracted for each participant, detrended, then deconvolved before being multiplied with the condition regressor (Face-Oval) to yield the interaction time-series. The interaction time-series, along with task condition and baseline regressors, were entered into a generalized least squares regression model that estimates the serial correlation of noise with an autoregressive moving average method, with correlation

coefficients and corresponding beta-weights as outputs of this model. The resulting correlation coefficients from the regression model were converted to z-scores using Fisher's transformation for the purposes of group analysis (see *Between-Group Emotion-Dependent Functional Connectivity Analysis* in the main text for details on the group analysis). Information on the resting-state analysis has been published previously (31) and can be found in the following section (*Resting-State Image Analysis*).

Resting-State Image Analysis

Functional image analysis was conducted using AFNI (32) and FSL (33). T1-weighted images were skull stripped using AFNI and transformed to MNI152 standard space using FLIRT (34, 35) followed by nonlinear alignment using FNIRT (36). The T1-weighted images were segmented into gray matter, white matter (WM) and cerebrospinal fluid (CSF) components using FSL's FAST (37). Prior to transformation to standard space, the WM mask was eroded by 1 voxel to reduce partial volume effects at the gray-white borders (38). EPI images were motion-corrected and aligned to the T1-weighted images in scanner space using a local Pearson correlation method (39). The time-series data were spatially blurred with a 4.2 mm full width at half maximum (FWHM) isotropic Gaussian filter kernel and subjected to global mean-based intensity normalization before being nonlinearly transformed to standard space (using the same matrix that transformed the T1-weighted images to MNI152 standard space). All subsequent analyses were thus conducted at $3 \times 3 \times 3$ mm resolution in standard space.

For our resting-state functional connectivity analysis, we used a generalized least squares regression model that estimates the serial correlation of noise with an autoregressive moving average method. To control for the effects of physiological processes (e.g., cardiac, respiratory),

we included the 6 motion parameters (3 rotational and 3 translational), their derivatives, and the mean signal from WM and CSF as nuisance regressors into the regression model (40). We opted not to include a global signal nuisance covariate in our model given the recent controversy regarding its use in resting-state analyses (40-43). Resting-state data have been shown to be particularly influenced by head motion (44); thus, we also applied rigorous motion outlier thresholds during preprocessing: volumes where the Euclidean norm of the 6 motion parameters were greater than 0.2 or where more than 10% of voxels were greater than the median absolute deviation of the detrended time-series were considered outliers and censored. Finally, bandpass filtering ($0.01 < f < 0.1$) was applied to the data via an inclusion of a series of sines and cosines into the regression model (31). This method of bandpass filtering, in addition to our nuisance regressors and our conservative censoring procedure (described above), therefore required a minimum number of 177 time points for our regression model to successfully fit the time-series data. Subjects whose preprocessed resting-state data did not meet this minimum threshold of time points for appropriate model fitting were therefore excluded from further analysis. Consequently, the data from 7 participants (4 MDD and 3 HCL) were excluded. We therefore report resting-state results for 57 subjects. More details on image analysis for the resting-state data can also be found in (31).

Comparisons with Prior Resting-State Data

Resting-state data from 11 of the 26 depressed adolescents and 30 of the 37 healthy controls in the present study have been previously published (31). However, the resting-state functional connectivity analyses in the present study used seeds based on emotionally-selective regions of the DMN and are therefore methodologically and anatomically distinct from the ones

used by Connolly and colleagues, which focused on portions of the anterior cingulate cortex defined based on *a priori* coordinates previously published (45). Moreover, one of the primary aims of the present study was to specifically examine emotion-dependent functional connectivity of the DMN since 1) emotional dysregulation is a key feature of MDD and 2) the role of the DMN more generally in adolescent depression is unclear. No work to date has explicitly examined the DMN during emotional processing in depressed adolescents. To our knowledge, there are only two studies examining functional connectivity of emotional processing in depressed adolescents (10, 46), and both are limited in their sample sizes (n = 14 per group in the paper by Perlman and colleagues and n = 19 per group by Ho and colleagues) and focus only on regions involved in salience and affective processing (e.g., amygdala, subcallosal cingulate gyrus). Thus, there is currently a gap in the literature regarding the role of the DMN specifically in adolescent depression. There has also been no work examining resting-state DMN connectivity in depressed adolescents until recently (47); however, this latest study reported no significant differences in resting-state DMN connectivity between depressed and never-disordered adolescents (47). Thus, the present study is the first to compare and report differences in emotion-dependent and resting-state functional connectivity of the DMN, as our prior resting-state study did not examine any task-based fMRI data whatsoever.

Between-Group Whole Brain Task Analysis

Several areas of the DMN were deactivated in HCL during emotional processing, including a large area of medial prefrontal cortex (mPFC) extending inferiorly into the pregenual anterior cingulate cortex (Table S2, Figure 2), left posterior cingulate cortex (PCC) (Table S2, Figure 2), and bilateral middle temporal gyri (Table S2, Figure S1). MDD failed to show

deactivation in these same regions during emotional processing and even exhibited hyperactivation in right parahippocampal and middle temporal clusters relative to HCL (Table S2, Figure S1). Moreover, activation in bilateral anterior insula was blunted in MDD compared to HCL (Table S2, Figure S1). Finally, MDD showed greater activation in visual processing regions (middle occipital cortex, lingual gyrus) compared to HCL (Table S2, Figure S1).

Controlling for Multiple Comparisons

All reported fMRI results were corrected at a whole brain level (cluster-wise $p < 0.05$). We computed the minimum number of contiguous voxels passing the voxel-wise threshold for a significant group difference ($F_{1,61} = 4.00$, $p = 0.05$) that would result in a cluster-wise $p < 0.05$ corrected threshold at the whole brain level using 10,000 iterations of Monte Carlo simulations.

Our simulations were based on an average skull-stripped whole brain mask comprising 24,511 voxels (661,797 µL) that overlapped with at least 90% of the slice stacks created from all our subjects and the imposed FWHM values (48). We used a first-nearest neighbor clustering method such that all above threshold voxels were considered part of a cluster if their faces touched. Based on our simulations, this minimum cluster threshold was 51 voxels (1377 µL).

An alternative method for estimating smoothness of functional data is to compute the FWHM values based on the individual residuals arising from the regression model in the first-level analysis (49, 50). However, this approach may not be appropriate when examining between-group effects and when the applied smoothing kernel is not three or more times larger than the voxel size, as is the case in the present study (48, 49, 51-53). As a comparison to our original approach, we estimated the smoothness of the functional data by averaging across all the individual residuals resulting from the first-level analysis. With these averaged FWHM values as

inputs into our Monte Carlo simulations, the alternative resultant cluster threshold was 65 voxels (1755 µL). Thus, all of the significant results reported in the main text survive this threshold except one – the subcallosal cingulate gyrus/lentiform nucleus region arising from the between-group PPI analysis with the PCC seed, which is 63 voxels (see Figure 4, Table 3 for more details). Given that several of the regions implicated in MDD are small in volume (e.g., subcallosal cingulate cortex, components of the striatum, limbic areas, etc), it is imperative to analyze fMRI data in a manner that is sensitive to detecting group differences in these structures, while at the same time optimally guarding against false positives. In the present study, we applied an appropriately sized smoothing kernel (54, 55) in conjunction with a conservative methodological approach to achieve these goals. Specifically, we employed a multiple regression model that accounts for the serial correlation of noise with an autoregressive moving average method at the first-level in combination with a linear mixed effects analysis that models subjects as random effects (and therefore more appropriately estimates variance in comparison to ANOVA or *t*-tests) at the group-level (56, 57). Thus, we feel confident that our methods take into account the variance between subjects and correlations between neighboring voxels while properly guarding against false positives.

Relating Emotion-Related Activation of mPFC and PCC with Elevated Emotion-Dependent Functional Connectivity

We correlated emotion-related activation of the mPFC and PCC with the emotion-dependent functional connectivity values from the areas exhibiting significant between-group differences in emotion-dependent functional connectivity of the respective seed (mPFC, PCC). The mPFC and PCC regions were those that resulted from the between-group whole brain task

results (see *Between-Group Whole Brain Task Analysis* in Methods section of the main text for more details). Emotion-related activation here is operationalized the percentage signal change computed from the Face-Oval linear contrast (see *Image Analysis* in the main text for more details). These mPFC and PCC regions were also used as seeds in the between-group emotion-dependent functional connectivity (PPI) analysis. For the purposes of this analysis, we operationalized functional connectivity as the beta-weights corresponding to the correlation coefficients resulting from our generalized least squares regression analysis when conducting the first-level PPI analysis (see *Emotion-Dependent Functional Connectivity (PPI) Image Analysis*, above, for more details). These beta-weights were extracted from each region exhibiting significant between-group differences in the PPI analysis. The correlations between emotion-related activation in the mPFC and PCC with each of these regions exhibiting significant between group differences in emotion-dependent functional connectivity of either the mPFC or PCC were conducted across the entire subject sample using two-tailed tests of the non-parametric Spearman's correlation coefficient (r_s). For a summary of the remaining correlational results, see Table S3.

Exploratory Analysis of Functional Connectivity

Emotion-dependent functional connectivity of mPFC and PCC seeds were performed as described in *Emotion-Dependent Functional Connectivity (PPI) Image Analysis* but with each emotion type as a condition regressor (i.e., Fear-Oval, Happy-Oval, Sad-Oval) in a distinct regression model. See Tables S4-S6 for a summary of the results from these exploratory analyses.

Examination of Psychosocial Treatment History

All depressed participants but 5 were either actively engaging in cognitive behavioral therapy, family therapy, or supportive therapy on a consistent basis (n = 18) or had done so at one point 3-4 years prior to the scan session (n = 3; see also Table S1). Using unpaired t-tests, we compared depressed subjects who were currently undergoing psychosocial therapies (n = 18) versus those who were not (n = 8) on depression rating scores, emotion-related activation in the mPFC and PCC seeds, and on functional connectivity values (i.e., Fisher's z-scores) in the clusters arising from the between-group PPI analysis. The mPFC and PCC regions were those that resulted from the between-group whole brain task results (see *Between-Group Whole Brain Task Analysis* in Methods section of the main text for more details). Emotion-related activation here is operationalized the percentage signal change computed from the Face-Oval linear contrast (see *Image Analysis* in the main text for more details). These mPFC and PCC regions were also used as seeds in the between-group emotion-dependent functional connectivity (PPI) analysis. Functional connectivity here is operationalized as Fisher's z-scores (see *Emotion-Dependent Functional Connectivity (PPI) Image Analysis*, above, for more details). The Fisher's z-scores were extracted from each region exhibiting significant between-group differences in the PPI analysis. We did not find any significant differences between depressed adolescents currently and not currently undergoing psychosocial therapies in BDI-II or Children's Depression Rating Scale-Revised depression scores (all p's > 0.2), brain activation in the mPFC and PCC (all p's > 0.27) nor in any of the functional connectivity values of the regions resulting from the between-group PPI analysis (all p's > 0.59). See Table S7 for a summary of these results.

Table S1. Summary of psychosocial treatment history in the depressed sample. All depressed subjects were medication-free except two: one ceased antidepressant usage 4 months before their brain scan and one ceased antidepressant usage 4 years before their brain scan.

Psychosocial Treatment	***n* (%)**
No Treatment	5 (19.23%)
Cognitive Behavioral Therapy (past, 3-4 years before scan)	2 (7.7%)
Family Therapy (past, 4 years before scan)	1 (3.8%)
Cognitive Behavioral Therapy (present)	10 (38.46%)
Family Therapy (present)	4 (15.38%)
Supportive Therapy (present)	4 (15.38%)

Table S2. Summary of location and size of significant clusters from the between-group whole brain task analysis. All results are corrected for multiple comparisons at a cluster-wise threshold of $p < 0.05$. Locations are reported according to the center of mass of cluster in Montreal Neurological Institute coordinates (radiological convention). See Figure S1 for more details and Figure 2 for more details on the seeds used for the psychophysiological interaction analysis.

Region (Brodmann's Area)	Location (x,y,z)	# of Voxels
Directionality: MDD > HCL		
L medial prefrontal cortex (BA 10/11), pregenual cingulate cortex (BA 24)	-4, 51, -2	350
L posterior cingulate cortex (BA 30)	-2, -51, 15	189
R parahippocampal cortex, amygdala, lentiform nucleus	27, -7, 5	170
R middle temporal gyrus (BA 21)	54, -6, -13	116
L middle temporal gyrus (BA 21)	-56, -13, -10	91
L lingual gyrus (BA 18)	-22, -88, -10	69
L middle occipital cortex (BA 19)	-42, -78, 6	57
Directionality: MDD < HCL		
R anterior insula (BA 13), inferior frontal gyrus (BA 47)	34, 23, 2	140
L anterior insula (BA 13), inferior frontal gyrus (BA 47)	-33, 21, 0	130

BA, Brodmann area; HCL, healthy controls; L, left; MDD, major depressive disorder; R, right.

Table S3. Correlations between emotion-related activation in the medial prefrontal cortex (mPFC) and posterior cingulate cortex (PCC) with psychophysiological interaction effect (beta-weights) across all subjects.

	Precuneus	**Cingulate Gyrus**	**Inferior Parietal Lobule Supramarginal Gyrus**
mPFC Seed	r_s = -0.010, p = 0.936	r_s = 0.148, p = 0.247	r_s = 0.204, p = 0.109
	Precuneus	**Cingulate Gyrus**	**Dorsal Striatum Subcallosal Cingulate Gyrus**
PCC Seed	r_s = -0.058, p = 0.654	r_s = 0.081, p = 0.527	r_s = 0.271, p = 0.032

Table S4. Regions showing significant between-group differences in fear-dependent functional connectivity. All results survived correction for multiple comparison at a cluster-wise $p < 0.05$. Locations are reported according to the center of mass of cluster in Montreal Neurological Institute coordinates (radiological convention). Fisher's z-scores are reported as mean ± SEM.

Region (Brodmann's Area)	Seed Region	MDD (Mean ± SEM)	HCL (Mean ± SEM)	Location (x,y,z)	# of Voxels
R Cingulate Gyrus, Postcentral Gyrus	mPFC	0.142 ± 0.023	0.071 ± 0.016	38, -18, 33	128
L Inferior Parietal Lobule	mPFC	0.150 ± 0.023	0.079 ± 0.017	-51, -19, 28	95
R Middle Temporal Gyrus (BA 21)	mPFC	-0.016 ± 0.014	0.059 ± 0.014	61, -30, -3	90
L Middle Temporal Gyrus (BA 21)	mPFC	0.026 ± 0.017	0.098 ± 0.011	-62, -26, -1	82
R Middle Temporal Gyrus (BA 21)	mPFC	-0.045 ± 0.011	0.026 ± 0.009	62, -10, -12	68
L Anterior Cingulate Cortex (BA 32)	mPFC	0.156 ± 0.028	0.067 ± 0.015	-3, 35, 28	63
R Medial Frontal Gyrus (BA 10)	mPFC	-0.026 ± 0.012	0.043 ± 0.008	19, 64, -3	60
L Supramarginal Gyrus	mPFC	0.132 ± 0.025	0.053 ± 0.016	-46, -54, 36	52
Precuneus (BA 7)	PCC	0.140 ± 0.022	0.058 ± 0.014	8, -68, 38	264
R Cingulate Gyrus (BA 31)	PCC	0.150 ± 0.022	0.069 ± 0.016	20, -37, 35	165
R Cingulate Gyrus, Postcentral Gyrus	PCC	0.142 ± 0.023	0.071 ± 0.016	38, -18, 33	128
L Supramarginal Gyrus	PCC	0.132 ± 0.025	0.053 ± 0.016	-46, -54, 36	52

BA, Brodmann area; HCL, healthy controls; L, left; MDD, major depressive disorder; mPFC, medial prefrontal cortex; PCC, posterior cingulate cortex; R, right.

Table S5. Regions showing significant between-group differences in happy-dependent functional connectivity. All results survived correction for multiple comparison at a cluster-wise $p < 0.05$. Locations are reported according to the center of mass of cluster in Montreal Neurological Institute coordinates (radiological convention). Fisher's z-scores are reported as mean ± SEM.

Region (Brodmann's Area)	**Seed Region**	**MDD (Mean ± SEM)**	**HCL (Mean ± SEM)**	**Location (x,y,z)**	**# of Voxels**
L Precuneus (BA 7/31)	mPFC	0.053 ± 0.009	0.007 ± 0.009	-7, -63, 33	92
L Superior Temporal Gyrus, Middle Temporal Gyrus	mPFC	0.044 ± 0.012	-0.004 ± 0.007	-36, 5, -30	74
R Subgenual Anterior Cingulate Cortex (BA 25), Orbitofrontal Gyrus (BA11)	mPFC	0.037 ± 0.007	-0.018 ± 0.007	5, 32, -16	56
Parahippocampal Cortex, Thalamus	PCC	0.051 ± 0.009	0.002 ± 0.008	-10, -24, -2	257
L Medial Frontal Gyrus (BA 11), Orbitofrontal Gyrus	PCC	0.039 ± 0.008	-0.010 ± 0.007	-4, 43, -14	225
R Lentiform Nucleus, Putamen	PCC	0.052 ± 0.01	0.001 ± 0.008	35, -28, -4	126
Precuneus (BA 7)	PCC	0.050 ± 0.01	0.003 ± 0.009	4, -68, 37	113
L Middle Temporal Gyrus (BA 21)	PCC	0.048 ± 0.01	0.000 ± 0.008	-62, -19, -11	92
R Middle Temporal Gyrus (BA 21)	PCC	0.059 ± 0.007	0.018 ± 0.007	52, 6, -19	84
R Fusiform Gyrus (BA 20)	PCC	0.037 ± 0.008	-0.003 ± 0.006	46, -16, -23	73
L Middle Temporal Gyrus (BA 21)	PCC	0.031 ± 0.008	-0.011 ± 0.006	-43, 5, -30	51

BA, Brodmann area; HCL, healthy controls; L, left; MDD, major depressive disorder; mPFC, medial prefrontal cortex; PCC, posterior cingulate cortex; R, right.

Table S6. Regions showing significant between-group differences in sad-dependent functional connectivity. All results survived correction for multiple comparison at a cluster-wise $p < 0.05$. Locations are reported according to the center of mass of cluster in Montreal Neurological Institute coordinates (radiological convention). Fisher's z-scores are reported as mean ± SEM.

Region (Brodmann's Area)	Seed Region	MDD (Mean ± SEM)	HCL (Mean ± SEM)	Location (x,y,z)	# of Voxels
L Parahippocampal Cortex, Amygdala	mPFC	0.070 ± 0.013	0.004 ± 0.014	-16, -10, -10	56
L Fusiform Gyrus	mPFC	0.058 ± 0.011	-0.002 ± 0.01	-28, -41, -20	51
R Middle Temporal Gyrus (BA 21), Superior Temporal Gyrus (BA 22)	PCC	0.031 ± 0.008	-0.016 ± 0.007	58, -24, -2	360
R Medial Prefrontal Cortex (BA 10)	PCC	0.044 ± 0.01	-0.006 ± 0.008	21, 54, 3	154
R Parahippocampal Cortex, Hippocampus	PCC	0.046 ± 0.01	-0.003 ± 0.008	25, -40, 1	65
L Caudate	PCC	0.029 ± 0.01	-0.018 ± 0.009	-17, 5, 24	65
R Superior Temporal Gyrus	PCC	0.022 ± 0.01	-0.021 ± 0.008	43, -50, -19	58
R Anterior Cingulate Cortex (BA 32)	PCC	0.017 ± 0.01	-0.030 ± 0.009	10, 46, 10	57

BA, Brodmann area; HCL, healthy controls; L, left; MDD, major depressive disorder; mPFC, medial prefrontal cortex; PCC, posterior cingulate cortex; R, right.

Table S7. Comparison of fMRI results between depressed subjects currently receiving psychosocial treatment (*n* = 18) versus those who are not (*n* = 8). For all depressed subjects, we extracted mean percentage signal change (Face-Oval) from the mPFC and PCC regions arising from the between-group whole brain task analysis (see *Methods* and Figure 2 the main text, as well as Table S2), and the mean functional connectivity (Fisher's z-scores) from all clusters arising from the between-group emotion-dependent functional connectivity analysis (see *Methods* and Tables 2-3 and Figures 3-4 in the main text for more details). We then compared these measurements between the MDD subjects currently undergoing psychosocial therapy and those who were not at the time of their scan. None of these results were statistically significant (all p's > 0.27). See also Table S1 for a detailed summary of the psychosocial treatment history of the depressed subjects.

Analysis	**Resulting Region of Interest**	**Statistic (t_{24})**
Between-group whole brain task analysis	mPFC (see Figure 2 and Table S2)	$t = 0.55$, $p = 0.59$
Between-group whole brain task analysis	PCC (see Figure 2 and Table S2)	$t = 0.04$, $p = 0.97$
Between-group PPI analysis with mPFC seed	Precuneus (see Figure 3, Table 2)	$t = 0.82$, $p = 0.42$
Between-group PPI analysis with mPFC seed	Cingulate gyrus (see Figure 3, Table 2)	$t = 1.12$, $p = 0.27$
Between-group PPI analysis with mPFC seed	Inferior parietal lobule/supramarginal gyrus (see Figure 3, Table 2)	$t = 0.98$, $p = 0.34$
Between-group PPI analysis with PCC seed	Precuneus (see Figure 4, Table 3)	$t = 0.19$, $p = 0.85$
Between-group PPI analysis with PCC seed	Cingulate gyrus (see Figure 4, Table 3)	$t = 0.64$, $p = 0.53$
Between-group PPI analysis with PCC seed	Dorsal striatum/subcallosal cingulate area functional connectivity (see Figure 4, Table 3)	$t = 0.04$, $p = 0.96$

MDD, major depressive disorder; mPFC, medial prefrontal cortex; PCC, posterior cingulate cortex; PPI, psychophysiological interaction.

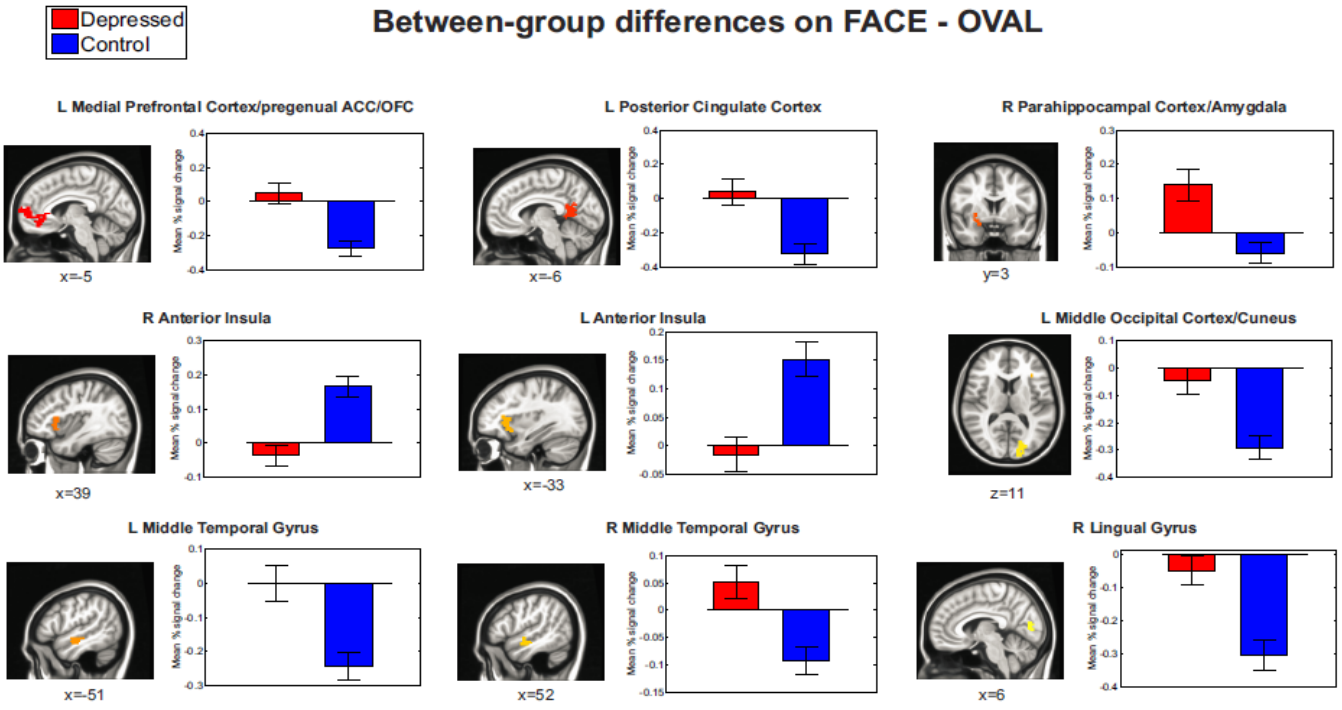

Figure S1. All regions showing significant between-group differences on the emotional identification task. All areas survived correction for multiple comparisons at a cluster-wise threshold of $p < 0.05$. Locations are reported in Montreal Neurological Institute coordinates (radiological convention). See Table S2 for more details. ACC, anterior cingulate cortex; L, left; OFC, orbitofrontal cortex; R, right.

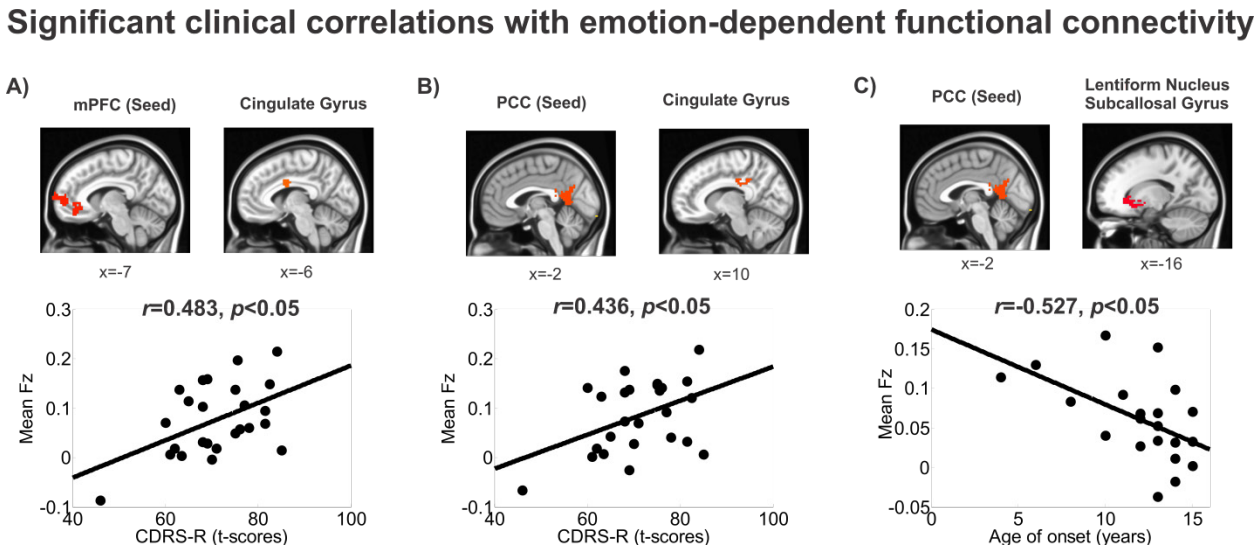

Figure S2. Summary of significant correlations between clinical variables and emotion-dependent functional connectivity. Within the major depressive disorder group only, the relationships between Children's Depression Rating Scale-Revised (CDRS-R), Beck Depression Inventory-II, Ruminative Responses Styles, Multidimensional Anxiety Scale for Children, and the mean Fisher's z-score within each of the significant regions identified by the between-group psychophysiological interaction analysis were examined with two-tailed tests of Pearson's correlation coefficient (*r*). The following relationships were significant: medial prefrontal cortex (mPFC)-cingulate gyrus and CDRS-R **(A)**, posterior cingulate cortex (PCC)-cingulate gyrus and CDRS-R **(B)**, and PCC-subcallosal gyrus and age of depression onset (**C**) Locations are reported in Montreal Neurological Institute coordinates (radiological convention).

Supplemental References

1. Shaffer D, Fisher P, Lucas CP, Dulcan MK, Schwab-Stone ME (2000): NIMH Diagnostic Interview Schedule for Children Version IV (NIMH DISC-IV): description, differences from previous versions, and reliability of some common diagnoses. *Journal of the American Academy of Child and Adolescent Psychiatry*. 39:28-38.

2. Lucas CP, Zhang H, Fisher PW, Shaffer D, Regier DA, Narrow WE, *et al.* (2001): The DISC Predictive Scales (DPS): efficiently screening for diagnoses. *Journal of the American Academy of Child and Adolescent Psychiatry*. 40:443-449.

3. Oldfield RC (1971): The assessment and analysis of handedness: the Edinburgh inventory. *Neuropsychologia*. 9:97-113.

4. Brown SA, Myers MG, Lippke L, Tapert SF, Stewart DG, Vik PW (1998): Psychometric evaluation of the Customary Drinking and Drug Use Record (CDDR): a measure of adolescent alcohol and drug involvement. *Journal of studies on alcohol*. 59:427-438.

5. Maxwell ME (1992): *Family Interview for Genetic Studies (FIGS): A manual for FIGS.* Rockville, MD: National Institute of Mental Health.

6. Tanner J (1962): Growth at Adolescence. 2nd. *Springfield: Charles C Thomas*.

7. Wechsler D (1999): *Wechsler Abbreviated Scale of Intelligence Administration and Scoring Manual*. San Antonio, TX: The Psychological Corporation.

8. Hollingshead A (1968): *Two factor index of social position (1957).* New York, New York: Wiley.

9. Sreenivas S, Boehm SG, Linden DE (2012): Emotional faces and the default mode network. *Neuroscience letters*. 506:229-234.

10. Ho TC, Yang G, Wu J, Cassey P, Brown SD, Hoang N, *et al.* (2014): Functional connectivity of negative emotional processing in adolescent depression. *Journal of affective disorders*. 155:65-74.

11. Stuhrmann A, Suslow T, Dannlowski U (2011): Facial emotion processing in major depression: a systematic review of neuroimaging findings. *Biology of mood & anxiety disorders*. 1:10.

12. Kerestes R, Davey CG, Stephanou K, Whittle S, Harrison BJ (2013): Functional brain imaging studies of youth depression: A systematic review. *NeuroImage Clinical*. 4:209-231.

13. Tao R, Calley CS, Hart J, Mayes TL, Nakonezny PA, Lu H, *et al.* (2012): Brain activity in adolescent major depressive disorder before and after fluoxetine treatment. *The American journal of psychiatry*. 169:381-388.

14. Norbury R, Selvaraj S, Taylor MJ, Harmer C, Cowen PJ (2010): Increased neural response to fear in patients recovered from depression: a 3T functional magnetic resonance imaging study. *Psychological medicine*. 40:425-432.

15. Norbury R, Mackay CE, Cowen PJ, Goodwin GM, Harmer CJ (2007): Short-term antidepressant treatment and facial processing. Functional magnetic resonance imaging study. *The British journal of psychiatry: the journal of mental science*. 190:531-532.

16. Stuhrmann A, Dohm K, Kugel H, Zwanzger P, Redlich R, Grotegerd D, *et al.* (2013): Mood-congruent amygdala responses to subliminally presented facial expressions in major depression: associations with anhedonia. *Journal of psychiatry & neuroscience : JPN*. 38:249-258.

17. Norbury R, Taylor MJ, Selvaraj S, Murphy SE, Harmer CJ, Cowen PJ (2009): Short-term antidepressant treatment modulates amygdala response to happy faces. *Psychopharmacology*. 206:197-204.

18. Fu CH, Williams SC, Brammer MJ, Suckling J, Kim J, Cleare AJ, *et al.* (2007): Neural responses to happy facial expressions in major depression following antidepressant treatment. *The American journal of psychiatry*. 164:599-607.

19. Fu CH, Mourao-Miranda J, Costafreda SG, Khanna A, Marquand AF, Williams SC, *et al. (*2008): Pattern classification of sad facial processing: toward the development of neurobiological markers in depression. *Biological psychiatry*. 63:656-662.

20. Surguladze S, Brammer MJ, Keedwell P, Giampietro V, Young AW, Travis MJ, *et al.* (2005): A differential pattern of neural response toward sad versus happy facial expressions in major depressive disorder. *Biological psychiatry*. 57:201-209.

21. Fu CH, Williams SC, Cleare AJ, Brammer MJ, Walsh ND, Kim J, *et al.* (2004): Attenuation of the neural response to sad faces in major depression by antidepressant treatment: a prospective, event-related functional magnetic resonance imaging study. *Archives of general psychiatry*. 61:877-889.

22. Fu CH, Williams SC, Cleare AJ, Scott J, Mitterschiffthaler MT, Walsh ND, *et al.* (2008): Neural responses to sad facial expressions in major depression following cognitive behavioral therapy. *Biological psychiatry*. 64:505-512.

23. Keedwell P, Drapier D, Surguladze S, Giampietro V, Brammer M, Phillips M (2009): Neural markers of symptomatic improvement during antidepressant therapy in severe depression: subgenual cingulate and visual cortical responses to sad, but not happy, facial stimuli are correlated with changes in symptom score. *Journal of psychopharmacology (Oxford, England)*. 23:775-788.

24. Keedwell PA, Drapier D, Surguladze S, Giampietro V, Brammer M, Phillips M (2010): Subgenual cingulate and visual cortex responses to sad faces predict clinical outcome during antidepressant treatment for depression. *Journal of affective disorders*. 120:120-125.

25. Costafreda SG, Khanna A, Mourao-Miranda J, Fu CH (2009): Neural correlates of sad faces predict clinical remission to cognitive behavioural therapy in depression. *Neuroreport*. 20:637-641.

26. LaBar KS, Crupain MJ, Voyvodic JT, McCarthy G (2003): Dynamic perception of facial affect and identity in the human brain. *Cerebral cortex (New York, NY : 1991)*. 13:1023-1033.

27. Sato W, Kochiyama T, Yoshikawa S, Naito E, Matsumura M (2004): Enhanced neural activity in response to dynamic facial expressions of emotion: an fMRI study. *Brain research Cognitive brain research*. 20:81-91.

28. Morris JS, Friston KJ, Buchel C, Frith CD, Young AW, Calder AJ, *et al.* (1998): A neuromodulatory role for the human amygdala in processing emotional facial expressions. *Brain : a journal of neurology*. 121 (Pt 1):47-57.

29. Ekman P, Friesen W (1976): *Pictures of Facial Affect.* Consulting Psychologists Press. Palo Alto, CA.

30. Perrett DI, May KA, Yoshikawa S (1994): Facial shape and judgements of female attractiveness. *Nature*. 368:239-242.

31. Connolly CG, Wu J, Ho TC, Hoeft F, Wolkowitz O, Eisendrath S, *et al.* (2013): Resting-state functional connectivity of subgenual anterior cingulate cortex in depressed adolescents. *Biological psychiatry*. 74:898-907.

32. Cox RW (1996): AFNI: software for analysis and visualization of functional magnetic resonance neuroimages. *Computers and biomedical research, an international journal*. 29:162-173.

33. Smith SM, Jenkinson M, Woolrich MW, Beckmann CF, Behrens TE, Johansen-Berg H, *et al.* (2004): Advances in functional and structural MR image analysis and implementation as FSL. *NeuroImage*. 23 Suppl 1:S208-219.

34. Jenkinson M, Smith S (2001): A global optimisation method for robust affine registration of brain images. *Medical image analysis*. 5:143-156.

35. Jenkinson M, Bannister P, Brady M, Smith S (2002): Improved optimization for the robust and accurate linear registration and motion correction of brain images. *NeuroImage*. 17:825-841.

36. Andersson JLR, Jenkinson M, Smith S (2007): Non-Linear Optimisation.

37. Zhang Y, Brady M, Smith S (2001): Segmentation of brain MR images through a hidden Markov random field model and the expectation-maximization algorithm. *IEEE transactions on medical imaging*. 20:45-57.

38. Jo HJ, Saad ZS, Simmons WK, Milbury LA, Cox RW (2010): Mapping sources of correlation in resting state FMRI, with artifact detection and removal. *NeuroImage*. 52:571-582.

39. Saad ZS, Glen DR, Chen G, Beauchamp MS, Desai R, Cox RW (2009): A new method for improving functional-to-structural MRI alignment using local Pearson correlation. *NeuroImage*. 44:839-848.

40. Fox MD, Zhang D, Snyder AZ, Raichle ME (2009): The global signal and observed anticorrelated resting state brain networks. *Journal of neurophysiology*. 101:3270-3283.

41. Anderson JS, Druzgal TJ, Lopez-Larson M, Jeong EK, Desai K, Yurgelun-Todd D (2011): Network anticorrelations, global regression, and phase-shifted soft tissue correction. *Human brain mapping*. 32:919-934.

42. Murphy K, Birn RM, Handwerker DA, Jones TB, Bandettini PA (2009): The impact of global signal regression on resting state correlations: are anti-correlated networks introduced? *NeuroImage*. 44:893-905.

43. Weissenbacher A, Kasess C, Gerstl F, Lanzenberger R, Moser E, Windischberger C (2009): Correlations and anticorrelations in resting-state functional connectivity MRI: a quantitative comparison of preprocessing strategies. *NeuroImage*. 47:1408-1416.

44. Power JD, Barnes KA, Snyder AZ, Schlaggar BL, Petersen SE (2012): Spurious but systematic correlations in functional connectivity MRI networks arise from subject motion. *NeuroImage*. 59:2142-2154.

45. Margulies DS, Kelly AM, Uddin LQ, Biswal BB, Castellanos FX, Milham MP (2007): Mapping the functional connectivity of anterior cingulate cortex. *NeuroImage*. 37:579-588.

46. Perlman G, Simmons AN, Wu J, Hahn KS, Tapert SF, Max JE, *et al.* (2012): Amygdala response and functional connectivity during emotion regulation: a study of 14 depressed adolescents. *Journal of affective disorders*. 139:75-84.

47. Pannekoek JN, van der Werff SJ, Meens PH, van den Bulk BG, Jolles DD, Veer IM, *et al.* (2014): Aberrant resting-state functional connectivity in limbic and salience networks in treatment-naive clinically depressed adolescents. *Journal of child psychology and psychiatry, and allied disciplines*.

48. Forman SD, Cohen JD, Fitzgerald M, Eddy WF, Mintun MA, Noll DC (1995): Improved assessment of significant activation in functional magnetic resonance imaging (fMRI): use of a cluster-size threshold. *Magnetic resonance in medicine.* 33:636-647.

49. Ledberg A, Akerman S, Roland PE (1998): Estimation of the probabilities of 3D clusters in functional brain images. *NeuroImage*. 8:113-128.

50. Kiebel SJ, Poline JB, Friston KJ, Holmes AP, Worsley KJ (1999): Robust smoothness estimation in statistical parametric maps using standardized residuals from the general linear model. *NeuroImage*. 10:756-766.

51. Xiong J, Gao JH, Lancaster JL, Fox PT (1995): Clustered pixels analysis for functional MRI activation studies of the human brain. *Human brain mapping*. 3:287-301.

52. Worsley KJ (1997): An overview and some new developments in the statistical analysis of PET and fMRI data. *Human brain mapping*. 5:254-258.

53. Petersson KM, Nichols TE, Poline JB, Holmes AP (1999): Statistical limitations in functional neuroimaging. II. Signal detection and statistical inference. *Philosophical transactions of the Royal Society of London Series B, Biological sciences*. 354:1261-1281.

54. White T, O'Leary D, Magnotta V, Arndt S, Flaum M, Andreasen NC (2001): Anatomic and functional variability: the effects of filter size in group fMRI data analysis. *NeuroImage*. 13:577-588.

55. Jones DK, Symms MR, Cercignani M, Howard RJ (2005): The effect of filter size on VBM analyses of DT-MRI data. *NeuroImage*. 26:546-554.

56. Mumford JA, Poldrack RA (2007): Modeling group fMRI data. *Social cognitive and affective neuroscience*. 2:251-257.

57. Poldrack RA, Mumford JA, Nichols TE (2011): *Handbook of functional MRI data analysis*. Cambridge University Press.